Metrol. Meas. Syst., Vol. 28 (2021) No. 1, pp. 73–88
DOI: 10.24425/mms.2021.135991

PAN POLSKA AKADEMIA NAUK

METROLOGY AND MEASUREMENT SYSTEMS
Index 330930, ISSN 0860-8229
www.metrology.wat.edu.pl

M&MS

A FILM STRESS MEASUREMENT SYSTEM APPLICABLE FOR HYPERBARIC ENVIRONMENT AND ITS APPLICATION IN COAL AND GAS OUTBURST SIMULATION TEST

Zhong-Zhong Liu[1,2)], Han-Peng Wang[1,2)], Liang Yuan[3)], Wei Wang[1,2)], Chong Zhang[1,2)], Yang Xue[1,2)]

1) *Shandong University, Geotechnical and Structural Engineering Research Centre, Jinan 250061, Shandong, China* (*201613331@mail.sdu.edu.cn*, ✉ *whp@sdu.edu.cn*, +86 531 8839 5428, *987067301@qq.com*, *zhangchong1970@163.com*, *577741462@qq.com*)
2) *Shandong University, School of Qilu Transportation, Jinan 250061, Shandong, China*
3) *Anhui University of Science and Technology, Huainan 232001, Anhui, China* (*1019895262@qq.com*)

Abstract

A film stress measurement system applicable for hyperbaric environment was developed to characterize stress evolution in a physical simulation test of a gas-solid coupling geological disaster. It consists of flexible film pressure sensors, a signal conversion module, and a highly-integrated acquisition box which can perform synchronous and rapid acquisition of 1 kHz test data. Meanwhile, we adopted a feasible sealing technology and protection method to improve the survival rate of the sensors and the success rate of the test, which can ensure the accuracy of the test results. The stress measurement system performed well in a large-scale simulation test of coal and gas outburst that reproduced the outburst in the laboratory. The stress evolution of surrounding rock in front of the heading is completely recorded in a successful simulation of the outburst which is consistent with the previous empirical and theoretical analysis. The experiment verifies the feasibility of the stress measurement system as well as the sealing technology, laying a foundation for the physical simulation test of gas-solid coupled geological disasters.

Keywords: stress measurement system, sealing technology, hyperbaric environment, coal and gas outburst, gas-solid coupling.

1. Introduction

In the fields of underground engineering and safety engineering, many engineering issues are related to gas-solid coupling. These issues involve interaction between gas and rock mass which is very complex. Coal and gas outburst is one of the typical gas-solid coupling geological hazards. A geomechanical model test is an effective method to study this kind of issues, but lack of a monitoring system is the key factor restricting the research [1–4].

Article history: received May 25, 2020; revised July 30, 2020; accepted October 1, 2020; available online February 9, 2021.

The detection technology used in the model test is very important for the test results. The sensors used not only need to meet the accuracy requirement, but also small size and good matching with the measured medium are required, so as to reduce the influence of the sensors themselves on the model test results. The earth pressure box is often used to obtain the value of internal stress of key positions in the model test. For example, Wang *et al.* [5] used an earth pressure box to study and analyze the variation law of stress-displacement of coal seam roof and explained a series of phenomena of coal seam roof collapse as well as summarized the influence factors of roof activity. Li *et al.* [6,7] used an earth pressure box to measure stress and explored the distribution of mining stress and the law of overburden failure in the process of coal seam mining. Zhang *et al.* [8] used an earth pressure box to measure the stress of gangue filling materials and analyze the evolution law of overburden fractures as well as discuss the impact of backfill mining on slowdown of overburden settlement. The main parameters of the state-of-art earth pressure sensors are collected in Table 1.

Table 1. Main parameters of three typical earth pressure sensors.

Item	**Resistance-type**	**Vibrating-wire type (single film)**	**Vibrating-wire type (double film)**
Sensitivity	0.05% F.S	0.1 % F.S	0.05 % F.S
Linearity	± 0.5% F.S	± 1.5% F.S	± 1% F.S
Resolution	≤ 0.05% F.S	≤ 0.2% F.S	≤ 0.05% F.S
Bandwidth	500 Hz	450 Hz	700 Hz
Detection limit	120% F.S	150% F.S	150% F.S
Accuracy	± 0.5% F.S	± 0.5% F.S	± 0.1% F.S
Compensation techniques	temperature self-compensated	temperature self-compensated	temperature self-compensated
Principle	piezoresistive effect	tension string theory	tension string theory

What is more, Tykhan *et al.* [9] proposed a new type of piezoresistive pressure sensors for environments with rapidly changing temperature. Bouřa *et al.* [10] proposed a wirelessly-powered high-temperature strain measuring probe based on piezoresistive nanocrystalline diamond layers, but the effect of applying an earth pressure box to test the pressure distribution proved unsatisfactory. The accuracy of test results was affected by its large size, too few test points, too much wiring, and stiffness greater than that of the measured medium. In addition, the mere existence of the earth pressure box affected the original stress field, especially one in the rock and soil around the pressure box, and changed the original distribution.

Besides earth pressure boxes, fiber grating sensors have been rapidly developed due to their small size, high sensitivity, being waterproof and resistant to electromagnetic interference as well as highly sensitive [11–17]. Chang *et al.* [18] designed and compared three kinds of fiber Bragg grating earth pressure sensors with different bonding modes. Wang *et al.* [19] developed a new type of a fiber Bragg grating earth pressure sensor for structural health monitoring which also performed temperature monitoring and self-compensation. Correia *et al.* [20] developed a fiber Bragg grating pressure sensor which can measure the earth pressure and pore pressure simultaneously. Hu *et al.* [21] designed a fiber Bragg grating earth pressure sensor with a hard center diaphragm as an elastic element. Li *et al.* [22] designed a fiber Bragg grating earth pressure sensor based on a double L-beam and applied it to earth pressure monitoring of a dam site. Hong et al. [23] developed a small soil deformation measurement system based on a fiber Bragg grating

Metrol. Meas. Syst., Vol. 28 (2021), No. 1, pp. 73–88
DOI: 10.24425/mms.2021.135991

for underground displacement monitoring. Xu *et al.* [24] constructed a soft fiber Bragg grating strain sensor which has the advantage of high precision and a small size and can be used for monitoring the subsurface deformation of the slope model. Piao *et al.* [25] used a fiber Bragg grating to study the deformation characteristics of overburden in the process of coal seam backfill mining and analyze the correlation between filling material and overburden settlement. In most of these studies, mechanical structures are used to convert the uniform pressure into the axial strain of a fiber Bragg grating. The sensitivity of the sensor is improved effectively, but at the same time deviation will be introduced, which will affect the consistency and stability of the sensor. Also, the sensor element is precise and fragile, so it cannot be used in hyperbaric gas-solid coupling model tests.

In addition to the choice of the sensor, the performance of the sealing of the signal wire and the protection of the sensor converter are the key parameters for data acquisition and the success rate of the hyperbaric gas-solid coupling model test. There are few previous studies on this, and the representative research results are as follows. Gao *et al.* [26] created a sealing sub-system and used a box to seal the lead, whose thickness was 30 ~ 35 cm, with two "O"-type sealing rings and high-strength bolts used for fastening the seal. Zhang *et al.* sealed the sensor signal wire using a sealing gasket in an outburst simulation test triggered by instant coal-seam uncovering. These studies only focused on the seal of signal wire but ignored the protection of the sensor converter and a simulation test triggered by tunneling under hyperbaric condition has never been reported.

In summary, the response frequency of the existing pressure sensors is low, and the maximum for a full bridge pressure box is only a few hundred Hz, which cannot meet the needs of data collection for an instantaneous stress change in an outburst test. The existing pressure sensors are difficult to be used in a hyperbaric gas-solid coupling model test due to their volume, stiffness, survival rate and pressure resistance. Nor can they meet the requirements of the sealing quality of the sensor signal wire. Based on this, a film stress measurement system and its sealing technology are proposed. Firstly, the film stress measurement system is introduced including the testing principle and functional characteristics of the sensor, the working principle of the signal conversion module and the pressure calibration of the sensor. Secondly, a sealing technology of this system under a high gas pressure environment is independently developed. Finally, its feasibility is tested in a large-scale coal and gas outburst model test triggered by tunneling under hyperbaric conditions.

2. The film stress measurement system

2.1. Testing principle of the sensor

In this paper, the principle behind the film pressure sensor is the piezoresistive effect in polysilicon. The piezoresistive effect was first discovered by Lord Kelvin in 1856. It is a phenomenon of obvious changing of resistance of materials under mechanical stress. When a solid material is affected by a force, the crystal lattice will deform and the carrier will scatter from one energy valley to another which will change the mobility of the carrier and disturb the average value of the carrier in the longitudinal and transverse direction and, in result, change the resistivity of the material.

The film pressure sensor is composed of two very thin polyester films. The inner surface of the two films is covered with a polysilicon resistance material. When the material is under pressure, its resistivity changes, and the electrical signal output proportional to the force change can be obtained through the measurement circuit of the provided signal conversion module.

2.2. Sensor features

The features of the film pressure sensor in this paper are as follows: (1) its thickness is only 0.1 mm; (2) it is flexible. It can fit the surface of the measured medium tightly had has a good adaptability; (3) the sensor wiring is small and fine, which can reduce the disturbance to the surrounding rock and soil. The physical and dimensional pictures of the sensor are shown in Fig. 1.

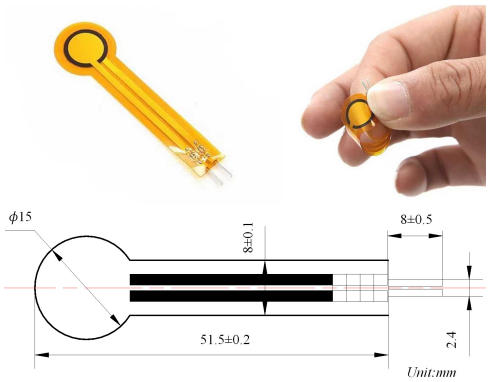

Fig. 1. The physical and dimensional pictures of the sensor.

2.3. Working principle of signal conversion module

The resistance-voltage conversion module is composed of a DC regulated power supply (VCC), a filter capacitor, a number of fixed-value resistors and an *analog-to-digital converter* (ADC). Through the circuit design and voltage sharing principle as shown in Fig. 2, the relationship between the resistance value of the film pressure sensor and the voltage at both ends of the fixed value resistance can be obtained:

$$\frac{Rx + R1}{R1} = \frac{U2}{U1}, \tag{1}$$

where, R_x is the resistance value of the sensor, R_1 is the fixed-value resistance, U_1 is the voltage value at both ends of the fixed value resistance, U_2 is the supply voltage value of the resistance-voltage conversion circuit (VCC), V.

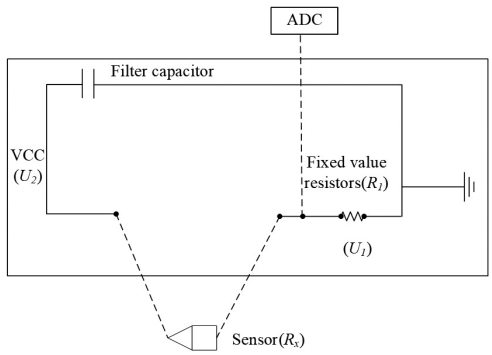

Fig. 2. Circuit design and the voltage sharing principle.

Metrol. Meas. Syst., Vol. 28 (2021), No. 1, pp. 73–88
DOI: 10.24425/mms.2021.135991

The module realizes the conversion of the resistance signal and voltage signal. When the VCC is powered with a constant voltage, there is a functional relationship between R_x and U_1 as shown in Eq. (1). The value of R_x can be calculated by measuring U_1, and the pressure value of the sensor can be obtained.

2.4. Pressure-voltage calibration

Pressure is applied on a single film pressure sensor with a push-pull machine and its value changes in the range of 0 ~ 500 N. Then, different pressure values of film pressure sensor and the output voltage values of the ADC are recorded. Finally, the relationship curve between the pressure of film pressure sensor and the output voltage of the ADC is obtained (Fig. 3).

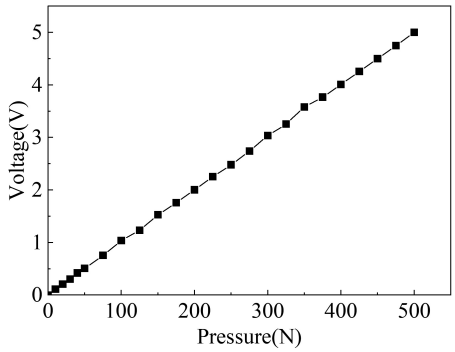

Fig. 3. Curve between the pressure and the output voltage.

2.5. Main parameters of the signal conversion module

The external dimensions of the conversion module are 1.4×3.2 cm (± 1mm), the power supply is 3.3 ~ 5 V, the output voltage range is 0 ~ 5 V, the accuracy of the conversion module is 1%, the conversion speed is 1 kHz, and interference-resistance is strong. There are corresponding interface identifications, among which the VCC is connected at 3 ~ 5 V voltage, GND is connected with a grounding wire, DO is the digital output interface and AO is the analog output interface. The module can match different models according to different sensor requirements, and the high-low level output under different pressures can be adjusted through the adjusting knob and the low-level indicator, as shown in Fig. 4.

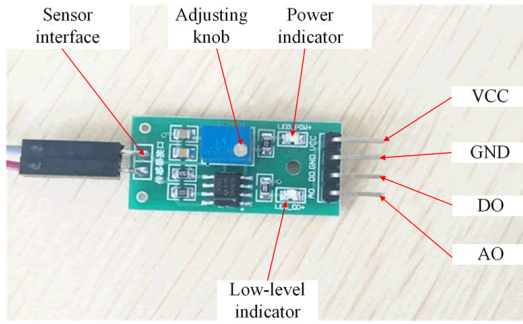

Fig. 4. Signal conversion module.

2.6. Highly-integrated acquisition module

The highly-integrated acquisition box and the supporting acquisition software can be connected with the gas pressure sensor, the temperature tensor, the stress sensor, and other sensors at the same time, as shown in Fig. 5. LabVIEW is used to compile the acquisition program to perform real-time synchronous acquisition of signals and visualization of test data. For the film pressure sensor and temperature sensor, the output mV level voltage signal is susceptible to interference. Therefore, a signal conversion module is needed to amplify the signal from the millivolt level to the volt level.

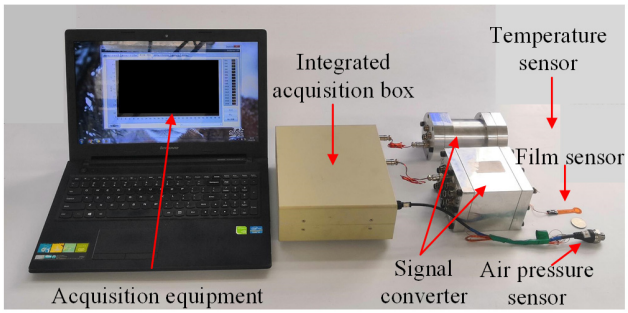

Fig. 5. Highly integrated acquisition module.

The key parameters of sensors and acquisition card are given in Table 2.

Table 2. Key parameters of sensors and acquisition card.

Stress sensor	Thickness	0.15 mm
	Response time	1 us
Conversion module of the stress sensor	Size	32 × 14 mm
	Speed	1 kHz
	Accuracy	± 1% FS
Temperature sensor	Size	0.15 × 0.25 mm
	Diameter	0.1 mm
	Range	−20–200°
Conversion module of the temperature sensor	Size	φ 44 × 21 mm
	Speed	1 kHz
	Accuracy	± 0.2% FS
Gas pressure sensor	Signal output range	0.5 – 4.5 V
	Accuracy	± 1.5% FS
Acquisition card	Channel number	16
	Sampling rate	500 kSa/s
	Input resolution	12 bit

Metrol. Meas. Syst., Vol. 28 (2021), No. 1, pp. 73–88
DOI: 10.24425/mms.2021.135991

3. Sealing technology in a hyperbaric gas environment

The sealing technology of the whole system includes the sealing of the sensor signal wire led out of the coal seam, the sealing and protection of the signal conversion module, and the sealing of the signal wire led out of a reaction apparatus. The overall connection mode and principle are shown in Fig. 6 and the details of the hyperbaric resistant sealing protection technology are shown in Fig. 7.

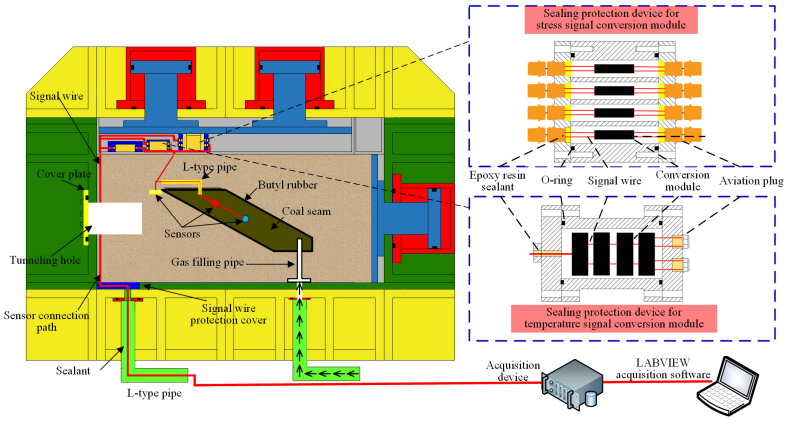

Fig. 6. The overall connection mode and principle.

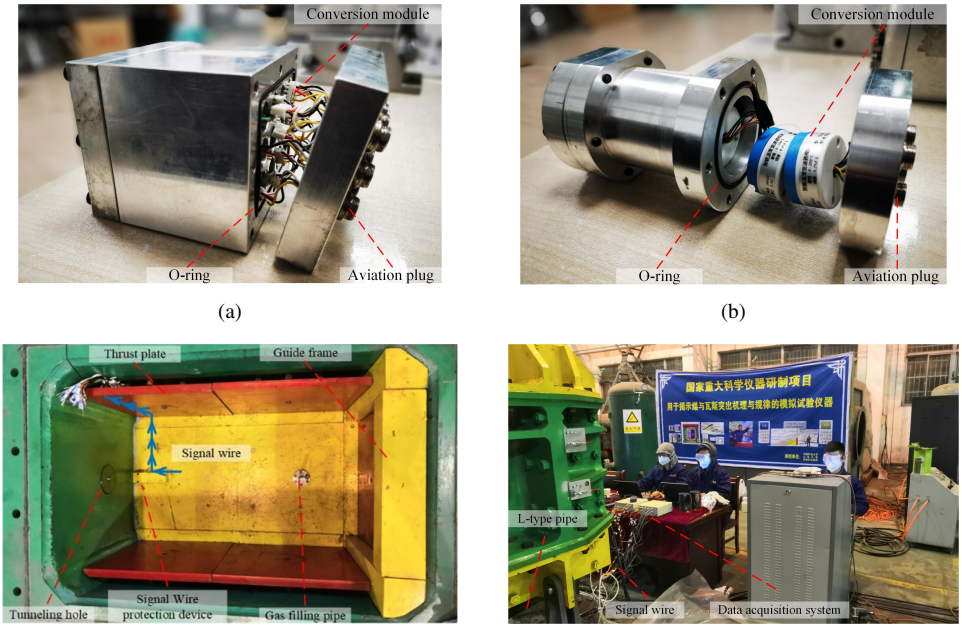

Fig. 7. Details of the hyperbaric resistant sealing protection technology. a) Sealing device for signal conversion module of film sensor. b) Sealing device for signal conversion module of temperature sensor. c) Signal wire arrangement inside the apparatus. d) Signal wire arrangement outside the apparatus.

3.1. Sealing technology of sensor signal wire led out coal seam

In the gas-solid coupling test, a good method to lead the sensor signal wire out of the coal seam and ensure the sealing effect is the key to the success of the test. In this paper, the following technical methods were adopted: a smooth enameled wire without outer insulation was adopted as the sensor signal wire and it was passed through the L-type pipe shown in Fig. 6, which was sealed with an epoxy resin sealant. The epoxy resin sealant mentioned in this paper is a two-component high temperature-resistant adhesive based on epoxy resin which is composed of epoxy resin A and hardener B mixed in a certain proportion. The ratio of A and B is 2.5:1 by volume. While being laid in the coal seam, the sensor was buried in a given position. One end of the L-type pipe was buried in the coal seam and then the coal seam and the L-type pipe was wrapped in butyl rubber. In the contact part between the L-type pipe and butyl rubber, the thickness was increased and a softening treatment was conducted to ensure the sealing effect. The outer side of butyl rubber was filled with rock-like material and the physical and mechanical parameters of the material could be precisely adjusted by matching the proportions of raw materials: the density was mainly affected by the moulding pressure and binder content, the uniaxial compressive strength and modulus of elasticity were mainly controlled by the moulding pressure, and the permeability of the material is mainly affected by the binder content. The density ranged from 2.323 g/cm^3 to 2.462 g/cm^3, the uniaxial compressive strength ranged from 4.16 MPa to 8.8 MPa, the modulus of elasticity ranged from 350 MPa to 1400 MPa, and the permeability ranged from 1×10^{-3} mD to 460×10^{-3} mD.

3.2. Sealing and protection of the signal conversion module

As hyperbaric gas in the gas-solid coupling model test can destroy the electronic components in the signal conversion module, we independently developed a hyperbaric sealing protection device to isolate the conversion module from the hyperbaric test environment (as shown in Fig. 6). The specific sealing principle is that the conversion module is put in the sealing device and its two ends are connected with an aviation plug and socket. The connections between the sensor, the conversion module and the acquisition device are realized through the male and female aviation plug. The key problem to be solved here is the sealing between the two end covers of the sealing device and the main body of the device, as well as the sealing of the thread of the aviation plug and socket. In order to solve this problem, O-rings and bolts are used to fasten and seal the end cover and the main body of the device, and epoxy resin sealant is poured into the air plug and the end cover for sealing. Through this sealing method, not only the protection and sealing of the conversion module are realized, but also the collection of test data is facilitated.

3.3. Sealing of the signal wire led out of the reaction apparatus

In order to solve the sealing problem of the signal wire led out of the reaction apparatus, an L-type pipe shown in Fig. 6 is designed. The sensor signal wire is passed through the L-type pipe and epoxy resin sealant is used for sealing. The L-type pipe not only facilitates the filling of the sealant, but also ensures the sealing effect after the sealant solidifies. During the test, the L-type sealing pipe is installed on the reaction frame through a flange, and an O-ring is used to seal the space between the flange and the reaction frame. One end of the sensor signal wire enters the reaction frame and is connected with the aviation socket on the signal amplifier sealing device, and the other end is connected with the information acquisition system outside the apparatus.

Metrol. Meas. Syst., Vol. 28 (2021), No. 1, pp. 73–88
DOI: 10.24425/mms.2021.135991

4. Test application

A coal and gas outburst is an extremely complex dynamic disaster in the process of underground coal mining. It is a typical gas-solid coupling problem which seriously threatens the safety of coal production [27, 28]. In order to verify the feasibility of the film pressure test system and its hyperbaric resistant sealing protection technology, a model test of coal and gas outburst induced by roadway excavation with a similar scale of 1/30 was carried out.

4.1. Test prototype and related parameters

The coal and gas outburst in a mine of the Huainan Mining Group is selected as the prototype. Considering the similarity criterion of physical simulation of a coal and gas outburst [29] as well as its geometric size, strength, rigidity and tightness of the test apparatus, the relevant test parameters were determined, as shown in Table 3.

Table 3. Test parameters.

Items	Values
Coal seam thickness (cm)	15
Coal seam dip (°)	30
Tunnel diameter (mm)	133
Back stress (MPa)	0.39
Lateral stress (MPa)	0.26
Upper stress (MPa)	0.39
Gas pressure (MPa)	1.1

4.2. Test apparatus

The test apparatus contains the coal and gas outburst simulation test instrument developed by the authors. The apparatus is divided into five key units as shown in Fig. 8. Among them,

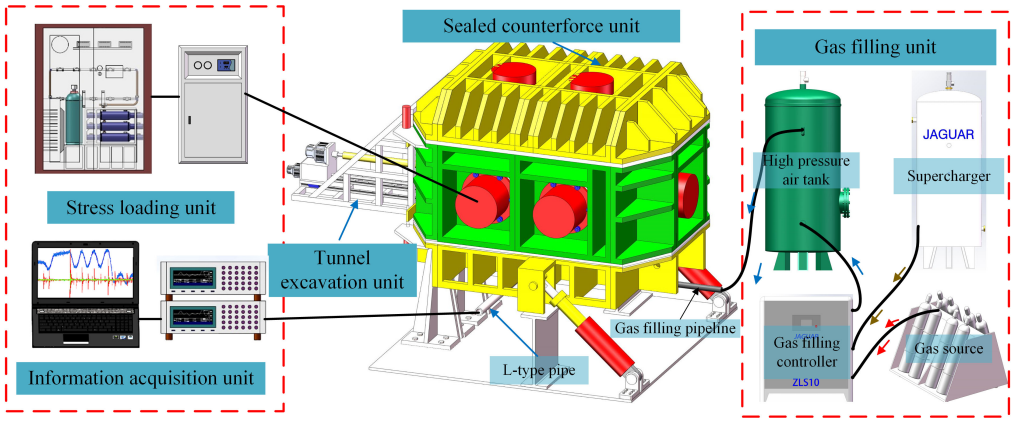

Fig. 8. Coal and gas outburst simulation test apparatus.

a sealed counterforce unit can provide the hyperbaric gas environment for the model. The external dimensions of the sealed counterforce unit are 2,030 mm × 2,170 mm × 2,030 mm. The dimensions of the internal model are 1,300 mm × 730 mm. From bottom to top, the counterforce device consists of a floor structure, a middle annular structure, and a roof structure. Each of these structures is produced by welding Q345 steel plates. The stress loading unit can faithfully simulate the ground stress environment. The gas filling unit can provide the maximum 5 MPa gas source for the experimental model. The tunnel excavation unit can perform tunnel excavation in the model. The information acquisition unit can collect the internal physical information of the model in real time.

4.3. Sensor arrangement

This test focused on the stress field and gas field on the roof of the tunnel as well as the stress field, gas field and temperature field of the coal seam. Therefore, film pressure sensors, gas pressure sensors, and temperature sensors were placed on the top of the tunnel and coal seam. The arrangement of some key sensors is shown in Fig. 9.

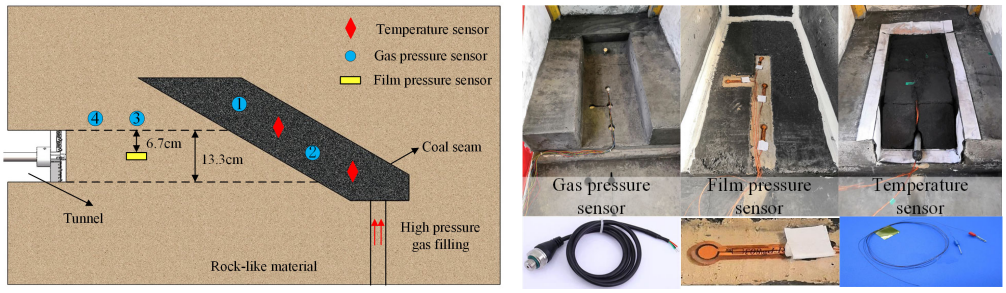

(a) (b)

Fig. 9. Arrangement of some key sensors. a) Locations of selected key sensors. b) Sensor placing.

4.4. Test process

The test process mainly includes model making, during which the coal seam space was limited using a wood form, sensor placing, apparatus unit debugging, geostress loading, filling the gas and maintaining pressure in the coal seam, tunnel excavation and multi-physical field information collection, as shown in Fig. 10.

4.5. Results and discussion

A violent coal and gas outburst phenomenon occurred when the tunneling distance reached 49.1 cm with a horizontal distance of 30 mm and a vertical distance of 1.5 cm between the tunneling face and the coal seam.

The test finally produced a violent coal and gas outburst after the cutter head had excavated 1.5 cm from the coal seam. The experimental phenomenon is very similar to the original coal and gas outburst phenomenon as shown in Fig. 11.

With the advance of the tunneling face, the collected geostress of the rock mass in front of the tunneling face collected by the film pressure sensor and the curve change are shown in Fig. 12.

Metrol. Meas. Syst., Vol. 28 (2021), No. 1, pp. 73–88
DOI: 10.24425/mms.2021.135991

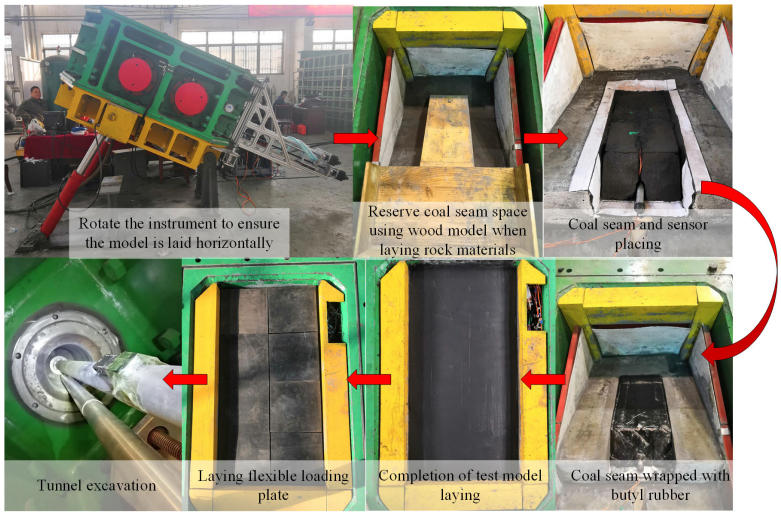

Fig. 10. The main test processes.

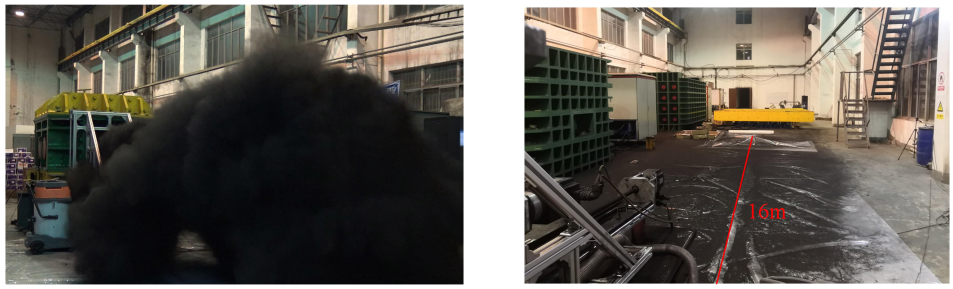

(a) (b)

Fig. 11. Coal and gas outburst phenomenon of the test. a) Photo of the coal and gas outburst. b) Pulverized coal thrown out during the test.

When the tunneling face is advancing normally, the overburden load of the goaf space transfers to the front of the tunneling face, making the vertical stress of the coal and rock mass in a certain range in front of the tunneling face greater than the original vertical stress [30, 31]. Under the action of support pressure, part of rock mass in the support pressure area (concentrated stress area) is damaged. After the failure, it continues to bear the pressure its residual strength. The area where the strength failure has occurred is called the limit equilibrium area of support pressure (plastic area), as shown in Fig. 13.

In this test, the rock mass is located in the protolith stress area and the concentrated stress area successively, which is consistent with the theoretical analysis, but there is no distressed area. The reason is that the strength of the surrounding rock in this test is 4.14 MPa which is far greater than the stress concentration value of the surrounding rock (1.35 MPa).

For linear elastic surrounding rock, the maximum compressive stress of a circular tunnel in non-uniform stress field appears around the surrounding rock. Because the strength of similar materials in the surrounding rock in this test is far greater than the vertical stress, it can be

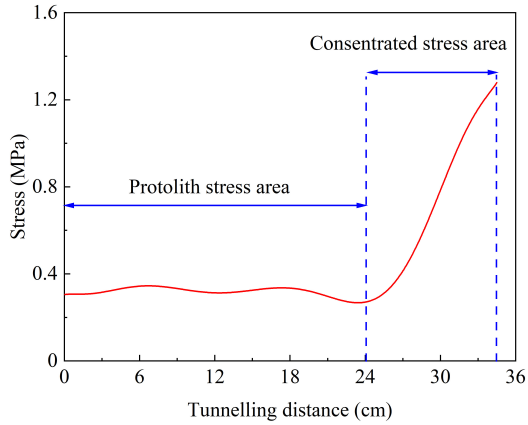

Fig. 12. Geostress curve in front of the tunneling face.

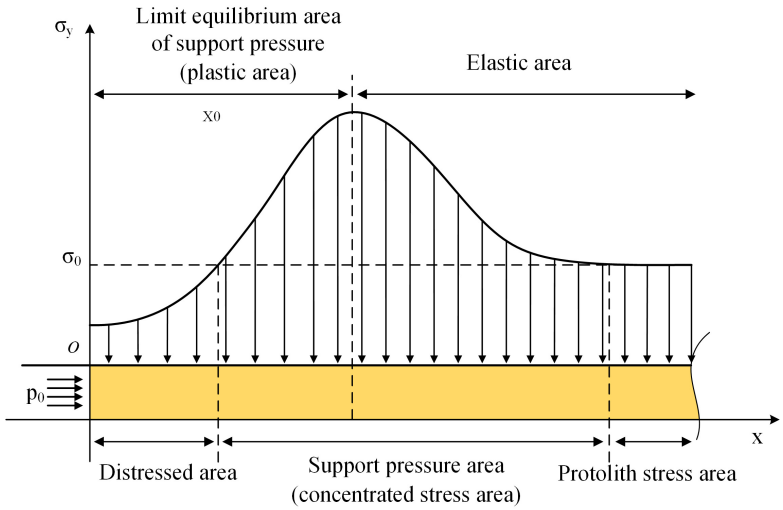

Fig. 13. Support pressure area in front of the tunneling face.

approximately considered as linear elastic surrounding rock. When the driving face is pushed to the location of the sensor, the surrounding rock stress at this position reaches the peak value (1.35 MPa), and the stress distribution law for a circular tunnel close to the tunneling face is consistent with the theoretical analysis.

In the test, the vertical stress in the original rock stress area is 0.36 MPa, which is the same as the vertical stress loading value. The peak value of the vertical stress in the stress concentration area is 1.35 MPa, which is 3.75 times bigger than the original rock stress. According to [32], the peak value of supporting pressure is 2 ~ 4 γH and the stress distribution in this test is consistent with it.

In the actual working conditions, during the process of tunnel excavation, the gas in the coal seam is sealed by the low-permeability roof and floor rock. At this time, although the roof and

Metrol. Meas. Syst., Vol. 28 (2021), No. 1, pp. 73–88
DOI: 10.24425/mms.2021.135991

floor rock may have a slight gas leakage, the gas pressure in the coal seam remains constant due to the large amount of gas absorbed by the coal seam. At the same time, the closer the tunnel is, the closer the air pressure in the surrounding rock is to the atmospheric pressure. This test faithfully reproduced the above phenomena.

In the process of outburst, the air pressure in the coal seam decreases to atmospheric pressure after 0.77s. Due to the low permeability of the surrounding rock and the role of lead wire sealing, the air pressure in the surrounding rock of the tunnel decreases to atmospheric pressure after 34.7s, as shown in Fig. 14. The results reveal the characteristics of gas seepage in the surrounding rock mass of coal seam, and confirm the feasibility of the sealing technology again.

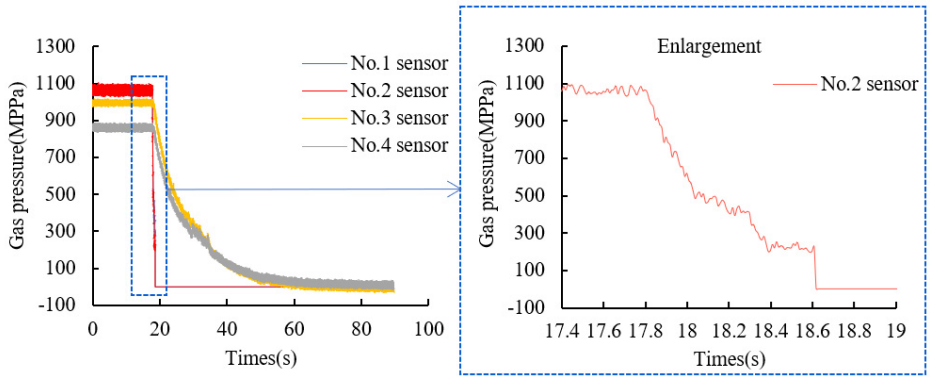

Fig. 14. Gas pressure change trend.

5. Conclusions

1. A new type of a film stress measurement system is proposed, which can be used in hyperbaric gas-solid coupling model tests. It consists of a flexible and bendable film pressure sensor, a signal conversion module, a highly integrated acquisition box and supporting acquisition software, which can perform the synchronous 1 kHz rapid acquisition of stress, air pressure and temperature signals.
2. A sealing technology and a protection method for precision components applicable for large-scale gas-solid coupling test are proposed. Its sealing structure and implementation mode, described here in detail, improve the survival rate of the sensor as well as the success rate of the test and the accuracy of the results.
3. The whole system is applied in the simulation test of gas-solid coupling of a large-scale coal and gas outburst triggered by tunneling under loading, gas-filling, and maintained pressure conditions. The test results are consistent with the previous empirical and theoretical analysis, which verifies the feasibility of the film stress measurement system and its sealing technology.

Acknowledgements

This research was funded by the National Natural Science Foundation of China (51427804), Natural Science Foundation of the Shandong Province (ZR2017MEE023,2019GSF111036).

References

[1] Wang, C., Yang, S., Li, X., Li, J., & Jiang, C. (2019). Comparison of the initial gas desorption and gas-release energy characteristics from tectonically-deformed and primary-undeformed coal. *Fuel*, 238, 66–74. https://doi.org/10.1016/j.fuel.2018.10.047

[2] Li, S. C., Gao, C. L., Zhou, Z. Q., Li, L. P., Wang, M. X., Yuan, Y. C., & Wang, J. (2019). Analysis on the Precursor Information of Water Inrush in Karst Tunnels: A True Triaxial Model Test Study. *Rock Mechanics and Rock Engineering*, *52*(2), 373–384. https://doi.org/10.1007/s00603-018-1582-2

[3] Hu, Q., Zhang, S., Wen, G., Dai, L., & Wang, B. (2015). Coal-like material for coal and gas outburst simulation tests. *International Journal of Rock Mechanics and Mining Sciences*, *74*, 151–156. https://doi.org/10.1016/j.ijrmms.2015.01.005

[4] Yekrangi, A., Yaghobi, M., Riazian, M., & Koochi, A. (2019). Scale-Dependent Dynamic Behavior of Nanowire-Based Sensor in Accelerating Field. *Journal of Applied and Computational Mechanics*, *5*(2), 486–497. https://dx.doi.org/10.22055/jacm.2018.27302.1393

[5] Wang, C. J., Yang, S. Q., Li, X. W., Yang, D. D., & Jiang, C. L. (2018). The correlation between dynamic phenomena of boreholes for outburst prediction and outburst risks during coal roadways driving. *Fuel*, *231*, 307–316. https://doi.org/10.1016/j.fuel.2018.05.109

[6] Li, S. G., Zhao, P. X., Lin, H. F., Xiao, P., & Wei, Z. Y. (2015). Study on character of physical simulation similar material of coal-rock and gas solid-gas coupling. *Journal of China Coal Society*, *40*(01), 80–86, (*in Chinese*). https://doi.org/10.13225/j.cnki.jccs.2014.003

[7] Li, S. G., Lin, H. F., Zhao, P. X., Xiao, P., & Pan, H. Y. (2014). Dynamic evolution of mining fissure elliptic paraboloid zone and extraction coal and gas. *Journal of China Coal Society*, *39*(08), 1455–1462, (*in Chinese*). https://doi.org/10.13225/j.cnki.jccs.2014.9013

[8] Zhang, J. X., Sun, Q., Zhou, N., Haiqiang, J., Germain, D., & Abro, S. (2016). Research and application of roadway backfill coal mining technology in western coal mining area. *Arabian Journal of Geosciences*, *9*(10), 558. https://doi.org/10.1007/s12517-016-2585-5

[9] Tykhan, M., Ivakhiv, O., & Teslyuk, V. (2017). New type of Piezoresistive Pressure Sensors for Environments with Rapidly Changing Temperature. *Metrology and Measurement Systems*, *24*(1), 185–192. https://doi.org/10.1515/mms-2017-0010

[10] Bouřa, A., Kulha, P., & Husák, M. (2016). Wirelessly Powered High-Temperature Strain Measuring Probe Based on Piezoresistive Nanocrystalline Diamond Layers. *Metrology and Measurement Systems*, *23*(3), 437–449. https://doi.org/10.1515/mms-2016-0036

[11] Xu, M. G., Reekie, L., Chow, Y. T., & Dakin, J. P. (1993). Optical in-fibre grating high pressure sensor. *Electronics Letters*, *29*(4), 398. http://doi.org/10.1049/el:19930267

[12] Yang, X. F., Dong, X. Y., Zhao, C. L., Ng, J. H., Peng, Q. Z., Zhou, X. Q., & Chao, L. (2005). A temperature-independent displacement sensor based on a fiber Bragg grating. *Proceedings of SPIE - the International Society for Optical Engineering*, *5855*, 691–694. https://doi.org/10.1117/12.623406

[13] Zhao, Y., Yu, C. B., & Liao, Y. B. (2004). Differential FBG sensor for temperature-compensated high-pressure (or displacement) measurement. *Optics & Laser Technology*, *36*(1), 39–42. https://doi.org/10.1016/S0030-3992(03)00129-4

[14] Zrelli, A. (2019). Simultaneous monitoring of temperature, pressure, and strain through Brillouin sensors and a hybrid BOTDA/FBG for disasters detection systems. *IET Communications*, *13*(18), 3012–3019. https://doi.org/10.1049/iet-com.2018.5260

Metrol. Meas. Syst., Vol. 28 (2021), No. 1, pp. 73–88
DOI: 10.24425/mms.2021.135991

[15] Lv, H. F., Zhao, X. F., Zhan, Y. L., & Gong, P. (2017). Damage evaluation of concrete based on Brillouin corrosion expansion sensor. *Construction & Building Materials*, *143*, 387–394. https://doi.org/10.1016/j.conbuildmat.2017.03.122

[16] Zrelli, A., & Ezzedine, T. (2018). Design of optical and wireless sensors for underground mining monitoring system. *Optik - International Journal for Light and Electron Optics*, *170*, 376–383. https://doi.org/10.1016/j.ijleo.2018.04.021

[17] Sabokrouh, M., & Farahani, M. (2019). Experimental study of the residual stresses in girth weld of natural gas transmission pipeline. *Journal of Applied and Computational Mechanics*, *5*(2), 199–206. https://dx.doi.org/10.22055/jacm.2018.25756.1294

[18] Chang, C., Johnson, G., Vohra, S. T., & Althouse, B. (2020). Development of fiber Bragg-grating-based soil pressure transducer for measuring pavement response. *SPIE*, 2000:3986, 480–488. https://doi.org/10.1117/12.388139

[19] Wang, W. H., Zhou, X. L., Wu, W. N., Chen, J. H., He, S. L., Guo, W. F., Gao, J. B., Huang, S. X., & Chen, X. H. (2019). Monolithic Structure-Optical Fiber Sensor with Temperature Compensation for Pressure Measurement. *Materials*, *12*(4), 552. https://doi.org/10.3390/ma12040552

[20] Correia, R., Jin, L., Staines, S., Chehura, E., & Tatam, R. P. (2009). Fibre Bragg grating based effective soil pressure sensor for geotechnical applications. *Proceedings of SPIE - the International Society for Optical Engineering*, *7503*, 75030F-75030F-4. https://doi.org/10.1117/12.835751

[21] Hu, Z. X., Wang, Z. W., Ma, Y. B., & Zhang, J. (2010). Soil pressure sensor based on temperature compensation FBG. *Journal of Applied Optics*, *31*(01), 110–113. (*in Chinese*)

[22] Li, F., Du, Y. L., Zhang, W. T., & Li, F. (2013). Fiber Bragg grating soil-pressure sensor based on dual L-shaped levers. *Optical Engineering*, *52*(1), 4403. https://doi.org/10.1117/1.OE.52.1.014403

[23] Hong, C. Y., Zhang, Y. I., Yang, Y. Y., & Yuan, Y. (2019). A FBG based displacement transducer for small soil deformation measurement. *Sensors & Actuators A Physical*, *286*, 35–42. https://doi.org/10.1016/j.sna.2018.12.022

[24] Xu, H. B., Zheng, X. Y., Zhao, W. G., Sun, X., Li, F., Du, Y. L., Liu, B., & Gao, Y. (2019). High Precision, Small Size and Flexible FBG Strain Sensor for Slope Model Monitoring. *Sensors*, *19*(12), 2716. https://doi.org/10.3390/s19122716

[25] Piao, C. D., Wang, D., Kang, H., He, H., Zhao, C. Q., & Liu, W. Y. (2019). Model test study on overburden settlement law in coal seam backfill mining based on fiber Bragg grating technology. *Arabian Journal of Geosciences*, *12*(13), 1–9. https://doi.org/10.1007/s12517-019-4564-0

[26] Cao, J., Sun, H. T., Wang, B., Dai, L. C., Zhao, B., Wen, G. C., & Zhao, X. S. (2019). A novel large-scale three-dimensional apparatus to study mechanisms of coal and gas outburst. *International Journal of Rock Mechanics & Mining Sciences*, *118*, 52–62. https://doi.org/10.1016/j.ijrmms.2019.04.002

[27] Nie, B. S., Li, X. C. (2012). Mechanism research on coal and gas outburst during vibration blasting. *Safety Science*, *50*(4), 741–744. https://doi.org/10.1016/j.ssci.2011.08.041

[28] Li, H., Feng, Z. C., Zhao, D., Dong, D. (2017). Simulation experiment and acoustic emission study on coal and gas outburst. *Rock Mechanics and Rock Engineering*, *50*(8), 2193–2205. https://doi.org/10.1007/s00603-017-1221-3

[29] Zhang, Q. H., Yuan, L., Wang, H. P., Kang, J. H., Li, S. C., Xue, J. H., Zhou, W., & Zhang, D. M. (2016). Establishment and analysis of similarity criteria for physical simulation of coal and gas outburst. *Journal of China Coal Society*, *41*(11), 2773–2779, (*in Chinese*). https://doi.org/10.13225/j.cnki.jccs.2016.0571

[30] Hu, Q. T., Wen, G. C. (2013). Mechanics mechanism of coal and gas outburst. *Science Press*: Beijing.

[31] Wei, Y., Lin, B. Q., Cheng, Z., Li, X. Z., An, S. (2012). How in situ stresses and the driving cycle footage affect the gas outburst risk of driving coal mine roadway. *Tunneling and Underground Space Technology Incorporating Trenchless Technology Research*, *31*, 139–148. https://doi.org/10.1016/j.tust.2012.04.015

[32] Li, S. G. (2000). Movement of the surrounding rock and gas delivery in fully-mechanized top coal caving. *China University of Mining and Technology Press*.

Zhong-Zhong Liu is a Ph.D. candidate from Shandong University, China. He has co-authored 8 journal publications. His current research interests include seepage properties of gassy coal and the mechanism of coal and gas outburst.

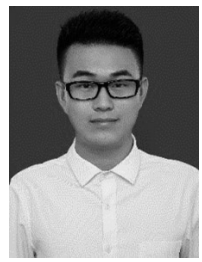

Wei Wang is a Ph.D. candidate from Shandong University, China. He has co-authored 3 journal publications. His current research interest is dynamic characteristics of coal rock.

Han-Peng Wang received the Ph.D. degree from Shandong University, China, in 2007. He is currently a Professor of the School of Qilu Transportation at Shandong University. He has co-authored 3 books, over 70 journal publications. His current research interest is the mechanism of coal rock dynamic disasters. His main research interests include pipeline inspection technology and safety evaluation, pipeline corrosion and protection, fluid transmission and control technology.

Chong Zhang is currently a Professor of the Geotechnical and Structural Engineering Research Centre in Shandong University. He has co-authored 1 book, over 20 journal publications. His current research interest is multi-information perception and acquisition.

Liang Yuan is an academician of the Chinese Academy of Engineering as well as President of the Anhui University of Science and Technology. He has co-authored 5 books, over 200 journal publications. His current research interest is coal and gas simultaneous extraction.

Yang Xue is a Ph.D. candidate from Shandong University, China. He has co-authored 3 journal publications. His current research interest is coal and gas exploitation.